

1 **A Case Study on Drivers of the Isotopic Composition**
2 **of Water Vapour at the Coast of East Antarctica**

3 **Rigo Chaar^{1,*}, Armin Sigmund^{1,*}, Pirmin Philipp Ebner², Michael Lehning^{1,3}**

4 ¹CRYOS, School of Architecture, Civil and Environmental Engineering, EPFL, Lausanne, Switzerland

5 ²Geophysical Institute and Bjerknes Centre for Climate Research, University of Bergen, Bergen, Norway

6 ³WSL Institute for Snow and Avalanche Research SLF, Davos, Switzerland

7 *These authors contributed equally to this work

8 **Key Points:**

- 9 • Direct air mass advection from the ice sheet leads to strongly depleted vapour iso-
- 10 • topic compositions at a ship close to the Mertz glacier.
- 11 • Both isotopic distillation due to cloud formation and sublimation of surface snow
- 12 • drive the vapour isotopic composition over the ice sheet.
- 13 • Ocean evaporation can quickly overwrite the isotopic signature of air masses shortly
- 14 • before arrival at the ship.

Abstract

Stable water isotopes (SWIs) contain valuable information on the past climate and phase changes in the hydrologic cycle. Recently, vapour measurements in the polar regions have provided new insights into the effects of snow-related and atmospheric processes on SWIs. The purpose of this study is to elucidate the drivers of the particularly depleted vapour isotopic composition measured on a ship close to the East Antarctic coast during the Antarctic Circumnavigation Expedition in 2017. Reanalysis data and backward trajectories are used to model the isotopic composition of air parcels arriving in the atmospheric boundary layer (ABL) above the ship. A novel approach is developed to account for moisture exchanges with the snow surface. The model generally reproduces the observed trend with strongly depleted vapour $\delta^{18}\text{O}$ values in the middle of the 6-day study period. This depletion is caused by direct air mass advection from the ice sheet where the vapour is more depleted in heavy SWIs due to distillation during cloud formation. The time spent by the air masses in the marine ABL shortly before arrival at the ship is crucial as ocean evaporation typically leads to an abrupt change in the isotopic signature. Snow sublimation is another important driver because the air masses and the sublimation flux will differ substantially in their isotopic composition if the air masses cross the ocean-snow boundary or descend from higher atmospheric levels. Although our model makes strong simplifications, it is a useful and computationally efficient method for understanding SWI dynamics at polar sites.

Plain Language Summary

Stable water isotopes are useful to reconstruct historical temperature conditions from ice cores. This method is possible because phase changes of water alter the isotopic composition. For example, if an air mass cools down, forms clouds, and produces rain or snowfall, the water vapour preferentially loses heavy water molecules. This study aims to explain a remarkable vapour isotopic signal measured on a ship close to the East Antarctic coast during six days in 2017. We model the isotopic composition of air parcels along their pathways to the ship and develop a novel approach to represent moisture exchange with the snow surface. The modelled vapour isotopic composition at the ship reaches a distinct minimum, similar to the measurements, when the air parcels move directly from the ice sheet to the ship. As expected, the vapour isotopic composition is lower over the ice sheet than over the ocean, largely due to cloud formation. However, moisture uptake from the snow surface and from the ocean shortly before arrival at the ship can strongly and abruptly influence the isotopic signature of the air masses. Although our model is not perfect, it helps to improve the interpretation of isotope measurements at polar sites.

1 Introduction

Stable water isotopes (SWIs) are widely used as both tracers in the global hydrologic cycle (Koeniger et al., 2010; Elliot, 2014) and as climate proxies in ice cores (Lorius et al., 1979; Grootes et al., 1994; EPICA community members, 2004). Several processes affect the vapour and snow isotopic composition, starting from the process of ocean evaporation in the source region (Craig & Gordon, 1965; Merlivat & Jouzel, 1979), transport processes (Helsen et al., 2006), cloud formation and precipitation (Jouzel & Merlivat, 1984; Ciais & Jouzel, 1994), and post-depositional processes (Cuffey & Steig, 1998; Johnsen et al., 2001; Jouzel et al., 2003; Krinner & Werner, 2003; Helsen et al., 2005, 2007).

Isotopic fractionation during cloud formation gives rise to isotopic distillation of atmospheric vapour. As a result, snowfall and surface snow on the Antarctic Ice Sheet generally become more depleted in heavy SWIs with increasing distance from the coast and elevation (Masson-Delmotte et al., 2008). Isotopic fractionation also plays an important role in phase changes at the Earth's surface. While the fractionation effects are well understood in the case of ocean evaporation, they are subject of current research

65 in the case of snow sublimation. Traditionally, it was assumed that sublimation occurs
66 layer by layer without fractionation (Friedman et al., 1991; Neumann & Waddington,
67 2004; Town et al., 2008). However, recent experimental studies found evidence of frac-
68 tionation during sublimation. For example, Hughes et al. (2021) sampled near-surface
69 vapour and snow in northeast Greenland with a high temporal resolution on clear-sky
70 summer days. These measurements demonstrated that alternating periods of sublima-
71 tion and vapour deposition can lead to clear diurnal cycles in the vapour isotopic com-
72 position, which are consistent with changes in the snow isotopic composition. Similar
73 diurnal cycles in the vapour isotopic composition were reported for Dome C on the Antarc-
74 tic plateau and explained by local sublimation and vapour deposition (Casado et al., 2016).
75 These findings are supported by controlled experiments in cold laboratories, showing that
76 snow-vapour exchange at the surface and in the pore space alters the isotopic compo-
77 sitions of snow and vapour (e.g., Sokratov & Golubev, 2009; Ebner et al., 2017). Equi-
78 librium fractionation explains a large part of these SWI dynamics although changes in
79 d-excess in both vapour and surface snow indicate some influence of kinetic fractiona-
80 tion (Casado et al., 2016; Hughes et al., 2021; Wahl et al., 2021).

81 The isotopic composition of atmospheric vapour observed at a specific site is in-
82 fluenced by weather changes on different time scales. At Thule Air Base, coastal north-
83 west Greenland, Akers et al. (2020) observed a strong seasonal cycle in vapour isotopic
84 composition controlled by shifts in sea-ice extent, which define the distance to marine
85 moisture sources. Synoptic weather events led to variations over multiple days, super-
86 imposed on the seasonal cycle. At Syowa station, coastal East Antarctica, Kurita et al.
87 (2016a) also found a strong influence of synoptic weather systems, causing advection of
88 marine or glacial air masses with distinct isotopic signatures. At other coastal polar sites,
89 shifts between these air masses manifest themselves in pronounced diurnal cycles in the
90 vapour isotopic composition, at least in summertime high-pressure periods. An exam-
91 ple is Dumont d’Urville, coastal East Antarctica, where strong katabatic winds advect
92 dry air with strongly depleted $\delta^{18}\text{O}$ values from the interior of the ice sheet during the
93 coldest hours of the day (Bréant et al., 2019). Similar diurnal cycles can be observed at
94 Kangerlussuaq, southwest Greenland, where an ice-free strip of land alternately ex-
95periences katabatic winds and a sea breeze (Kopec et al., 2014).

96 Apart from measurements, models are an important tool for understanding the dy-
97 namics of SWIs in the atmosphere and the driving processes. There are two modelling
98 approaches: (1) Lagrangian models which simulate moist processes and isotopic fraction-
99 ation along air parcel trajectories (Jouzel & Merlivat, 1984; Ciais & Jouzel, 1994; Helsen
100 et al., 2006; Sinclair et al., 2011; Christner et al., 2017); and (2) Eulerian models, such
101 as general circulation models (GCMs), which consider the temporal change on a fixed
102 three-dimensional grid (e.g., Joussaume et al., 1984; Pfahl et al., 2012). Eulerian mod-
103 els provide a more accurate representation of the spatial variability of the isotopic com-
104 position of water vapour across the hydrologic cycle by accounting for the mixing of air
105 masses of different origins and the highly variable pathways water vapour may take be-
106 tween evaporation and condensation. For example, GCMs are able to satisfactorily re-
107 produce the global and seasonal variations in the isotopic composition of precipitation
108 (Noone & Sturm, 2010; Hoffmann et al., 2000). However, it is more difficult to discern
109 the effect of individual processes on isotopic variability using Eulerian models as these
110 processes can be isolated less easily, compared to the computationally more efficient La-
111 grangian models (Dütsch et al., 2018). Thurnherr et al. (2021) used a combination of
112 both approaches to better understand vapour isotopic measurements along the ship route
113 of the Antarctic Circumnavigation Expedition (ACE). The output of the Eulerian model
114 COSMO_{iso} was analyzed along backward trajectories starting at the position of the ship.
115 This method demonstrated that the cold and warm sectors of extratropical cyclones, as-
116 sociated with evaporation and dew formation, respectively, were important drivers of the
117 vapour isotopic composition over the open ocean.

118 In the present study, we develop a Lagrangian model to explain the vapour isotopic
 119 signal of a specific event during the ACE campaign. We investigate in detail a 6-day pe-
 120 riod in January 2017, in which the ship stayed close to the Mertz glacier, East Antarc-
 121 tica, and the values of vapour $\delta^{18}\text{O}$ reached a pronounced minimum. The objectives are
 122 to (i) reproduce the $\delta^{18}\text{O}$ values of water vapour observed at the Mertz glacier using a
 123 Lagrangian model with simple isotope dynamics and (ii) better understand the influences
 124 of air mass origin and isotopic fractionation during moisture exchange with the Earth's
 125 surface and during cloud formation. Our model accounts for equilibrium fractionation
 126 but neglects kinetic effects during all phase changes apart from ocean evaporation. As
 127 some other models still neglect isotopic fractionation during snow sublimation, we an-
 128 alyze how sensitive the modelled vapour $\delta^{18}\text{O}$ is with respect to the assumptions that
 129 snow sublimation is or is not associated with equilibrium fractionation. Although our
 130 model represents some processes less accurately than the COSMO_{iso}-based modelling frame-
 131 work of Thurnherr et al. (2021), we are able to directly distinguish the effects of indi-
 132 vidual processes with a lower computational effort. The novelty of our Lagrangian iso-
 133 tope model is the fact that it computes the isotopic composition of sublimating surface
 134 snow by accounting for the history of snowfall and surface-atmosphere exchange, con-
 135 sidering a multi-layer snowpack. The last aspect is an advantage over the COSMO_{iso} model,
 136 which treats the snowpack as a single homogeneous layer.

137 2 Data and Methods

138 2.1 Water Vapour Measurements at the Mertz Glacier

139 The ACE campaign took place between November 2016 and April 2017. A contin-
 140 uous time series of water vapour isotopic composition was recorded at the position of the
 141 ship at a height of approximately 13.5 m a.s.l. using a cavity ring-down laser spectrom-
 142 eter with a high temporal resolution of 1 s. More details and an overview of this time
 143 series can be found in Thurnherr, Kozachek, et al. (2020). Here, we focus on the period
 144 from 27th January to 1st February 2017 as it includes two consecutive days with excep-
 145 tionally depleted values of $\delta^{18}\text{O}$ and δD . This event occurred while the ship was anchored
 146 close to the outlet of the Mertz glacier and coincided with low values of specific humid-
 147 ity and high values of d-excess (Figure 5 in Thurnherr, Kozachek, et al., 2020), typical
 148 of continental Antarctic interior air masses (Bréant et al., 2019).

149 2.2 Modelling Approach

150 We developed a model, which considers the most common three SWIs (H_2^{16}O , H_2^{18}O ,
 151 HD^{16}O) although we only present $\delta^{18}\text{O}$ in the results. The model consists of two parts:
 152 (i) *Model Sublimation* computes the isotopic composition of surface snow, which deter-
 153 mines that of the sublimation flux; (ii) *Model Air Parcel* quantifies the vapour isotopic
 154 composition along air parcel trajectories, considering vapour exchange with the snow or
 155 ocean surface and vapour removal due to cloud formation (Figure 1). For the phase changes
 156 of snow sublimation, vapour deposition, and condensation, we only consider equilibrium
 157 fractionation as a first-order approximation and use temperature-dependent formulas for
 158 the fractionation factors from Merlivat and Nief (1967), Majoube (1970), and Majoube
 159 (1971). To evaluate the importance of fractionation during sublimation, we compare two
 160 simulations, which assume that snow sublimation is associated with equilibrium fraction-
 161 ation (Run E) or not associated with any fractionation (Run N). In both simulations,
 162 kinetic fractionation is only taken into account in the process of ocean evaporation by
 163 applying the widely-used Craig-Gordon formula in its original form (Craig & Gordon,
 164 1965; Horita et al., 2008).

165 The next sections explain the input data and main characteristics of the two model
 166 parts while further methodological details and equations can be found in Texts S1 to S3
 167 in the Supporting Information. Important model constants and parameters are listed in

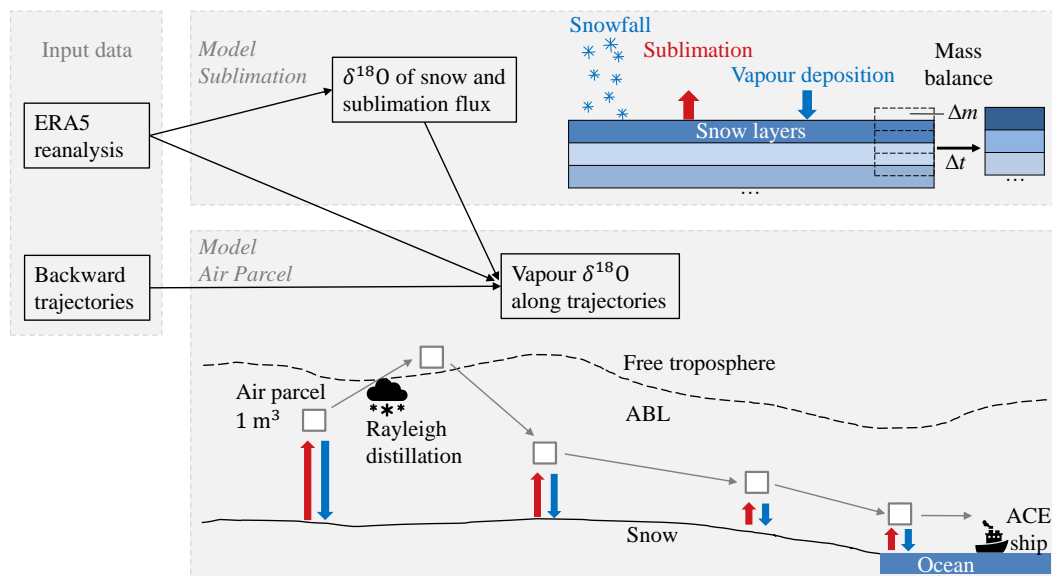


Figure 1. Schematic illustration of the modelling approach. The net accumulation of snow mass in one time step (Δt), denoted by Δm , may be positive or negative.

168 Table S1. For brevity, we refer to the surface water vapour flux as the surface flux from
 169 here on. All time information in this paper is given in UTC time while local time at the
 170 outlet of the Mertz glacier corresponds to UTC+10 h.

171 2.2.1 Input Data

172 The model uses ERA5 reanalysis data produced by the European Centre for Medium-
 173 Range Weather Forecasts (ECMWF) with spatial and temporal resolutions of $0.25^\circ \times$
 174 0.25° and 1 h, respectively (Hersbach et al., 2018). The following variables were retrieved:
 175 land-sea mask, mean snow evaporation rate (for grid cells with land fraction > 0.5 and
 176 latitude $< 60^\circ$ S), mean evaporation rate (for grid cells with land fraction ≤ 0.5 , con-
 177 sidered as liquid ocean surface), air temperature and dew point temperature at 2 m height,
 178 surface temperature, atmospheric pressure, and snowfall rate. Snow evaporation, i.e., sub-
 179 limation, and ocean evaporation are based on the common Monin-Obukhov bulk param-
 180 eterization assuming constant roughness lengths on the ice sheet ($z_{0m} = 0.0013$ m, $z_{0T} =$
 181 $z_{0q} = 0.00013$ m) and dynamic roughness lengths for the ocean depending on a wave
 182 model (ECMWF, 2016). In addition to the snow surface, drifting and blowing snow par-
 183 ticles contribute to the sublimation flux (Sigmund et al., 2021) and consequently they
 184 may change their isotopic composition. However, drifting and blowing snow is not rep-
 185 resented in the ERA5 reanalysis and there is little knowledge about isotopic effects of
 186 this process. In the main analysis, we use data for latitudes south of 30° S from July 2016
 187 to February 2017. The first six months serve as a spin-up period to reduce uncertain-
 188 ties arising from the initialisation of the snow isotopic composition. For purposes of val-
 189 idation, we compare results of *Model Sublimation* with isotope measurements at Dome
 190 C, East Antarctica, published by Casado et al. (2016, 2018). To this end, ERA5 data
 191 for the grid cell including Dome C (75° S, 123.25° E) and the period from January 2013
 192 to January 2016 are used.

193 *Model Air Parcel* additionally assimilates 10-day backward air parcel trajectories
 194 taken from Thurnherr, Wernli, and Aemisegger (2020). These trajectories were calcu-
 195 lated with the Lagrangian analysis tool LAGRANTO (Wernli & Davies, 1997; Sprenger

196 & Wernli, 2015) using the 3D-wind fields from the ECMWF operational analyses. Ev-
 197 ery hour, a set of trajectories was launched from up to 56 vertical levels between 0 and
 198 500 hPa above sea level along the ACE cruise track. For each trajectory, the time step
 199 was 3 h. In this study, the following variables were extracted for trajectories arriving at
 200 the ship in the period from 27th January to 1st February 2017: air pressure at heights
 201 of the air parcel and the ABL, specific humidity, and air temperature.

202 **2.2.2 Model Sublimation**

203 In the case of snow sublimation, the isotopic composition of the surface flux de-
 204 pends on that of the surface snow (e.g., Wahl et al., 2021). The latter is initialized with
 205 typical values for snowfall depending on the temperature and the effects of snowfall and
 206 surface flux on the snow isotopic composition are simulated with time. The snowfall $\delta^{18}\text{O}$
 207 is parameterized as a linear function of the daily running mean air temperature because
 208 in the literature, this relationship is derived from daily mean values. We apply the same
 209 linear function to snowfall over the whole Antarctic continent although different $\delta^{18}\text{O}$ -
 210 temperature slopes have been measured at different sites. In our baseline simulation, the
 211 function for snowfall $\delta^{18}\text{O}$ is taken from Stenni et al. (2016), henceforth Stenni16, and
 212 characterized by an intermediate slope of 0.45‰ K^{-1} . Sensitivity tests are performed
 213 using functions from Landais et al. (2012) and Fujita and Abe (2006), henceforth Landais12
 214 and FA06, respectively, with low and high slopes of 0.35‰ K^{-1} and 0.78‰ K^{-1} , respec-
 215 tively (Texts S2 and S4 in the Supporting Information).

216 The snowpack is modelled as a series of 100 layers, each with the same thickness
 217 and a constant density of 350 kg m^{-3} . For the location of Dome C, we tested three val-
 218 ues for the snow layer thickness (0.1 cm, 1 cm, and 10 cm) and compared the surface snow
 219 $\delta^{18}\text{O}$ with measurements of Casado et al. (2018). A thickness of 1 cm led to the best agree-
 220 ment and was therefore selected for the remaining analysis (Text S4 and Figure S1 in
 221 the Supporting Information). We assume that the snowpack always exists in grid cells
 222 south of 60° S with a land fraction greater than 0.5. If the snowfall and surface fluxes
 223 add or remove snow mass at the surface, a simple mixing mechanism will guarantee that
 224 the thickness and mass of the snow layers remain constant. More precisely, a part of each
 225 layer is mixed with an adjacent layer to compensate for the mass gain or loss at the sur-
 226 face (Figure 1). We neglect changes in snow density and assume that snow added by snow-
 227 fall or vapour deposition has the same density as the snowpack. The mixing mechanism
 228 is a vastly simplified version of a realistic vapour transport mechanism (Jafari et al., 2020).
 229 In reality, the interplay between ventilation, isotope diffusion within the snowpack and
 230 recrystallisation can cause a continuous replacement of the interstitial water vapour in
 231 the surface snow layer. However, it is still an open question how the combination of these
 232 processes can quantitatively change the isotopic compositions of snow and the water vapour
 233 in the ABL. Therefore, our model is based on the following assumptions: (1) no isotope
 234 diffusion within the snow layers; (2) no impact of snow metamorphism on the isotopic
 235 profile; (3) fractionation only at the uppermost snow layer because of its direct contact
 236 with the atmosphere; and (4) no ventilation within the snow layer.

237 In the case of vapour deposition, the isotopic composition of the surface flux de-
 238 pends on that of the atmospheric vapour. *Model Sublimation* estimates the latter as the
 239 mean of two hypothetical values for vapour, which is in isotopic equilibrium with the sur-
 240 face snow or with potential snowfall, respectively. This simple estimate accounts for the
 241 fact that both local snow sublimation and the distillation process during air mass trans-
 242 port can influence the vapour isotopic composition. However, the importance of both
 243 influences varies in reality depending on weather conditions. Figure S2b and Text S4 in
 244 the Supporting Information show that the simple estimate for vapour $\delta^{18}\text{O}$ reproduces
 245 the mean value measured by Casado et al. (2016) at Dome C in a 24-d period in aus-
 246 tral summer 2014/2015 (mean bias error of -0.2‰) although the temporal variability
 247 is strongly underestimated. On the basis of this comparison, we expect uncertainties of

248 a few ‰ in our simple estimate of the vapour isotopic composition. This estimate is only
 249 used to compute the effect of a limited amount of vapour deposition in *Model Sublima-*
 250 *tion* and to initialize some of the air parcels. Vapour deposition plays a limited role be-
 251 cause the total mass removed from all modelled air parcels due to vapour deposition is
 252 22 times lower than the total mass taken up by all parcels due to snow sublimation.

253 2.2.3 Model Air Parcel

254 We consider air parcels with a constant volume of $1 \times 1 \times 1 \text{ m}^3$, travelling along
 255 the trajectories that arrive within the ABL at the position of the ship. This criterion re-
 256 sults in 6 to 24 trajectories per arrival time and an average value of 13 trajectories. The
 257 isotopic composition of each air parcel is initialized when the parcel resides in the ABL
 258 for the first time. If this situation occurs over snow (land fraction $> 50 \%$ and latitude
 259 south of 60° S), the isotopic composition of the parcel will be initialized as a function
 260 of the isotopic compositions of surface snow and potential snowfall (same assumption
 261 as used in *Model Sublimation* for atmospheric vapour). Over the ocean, the parcel is only
 262 initialized when it is influenced by evaporation because this condition allows us to es-
 263 timate the initial isotopic composition of the parcel using the Craig-Gordon formula sim-
 264 plified with the global closure assumption (e.g. Dar et al., 2020). Under this assump-
 265 tion, the isotopic composition of atmospheric vapour equals that of the evaporate. If the
 266 trajectory crosses the ABL over land north of 60° S , the isotopic composition of the sur-
 267 face flux is not known and therefore the parcel will be initialized once over water or south
 268 of 60° S . An overview of the locations of initialization and the position of the ship is given
 269 in Figure 2. On average, the air parcels are initialized 5.3 days before arriving at the ship.
 270 The specific humidity of the parcel is initially taken from the trajectory data set and then
 271 modelled explicitly.

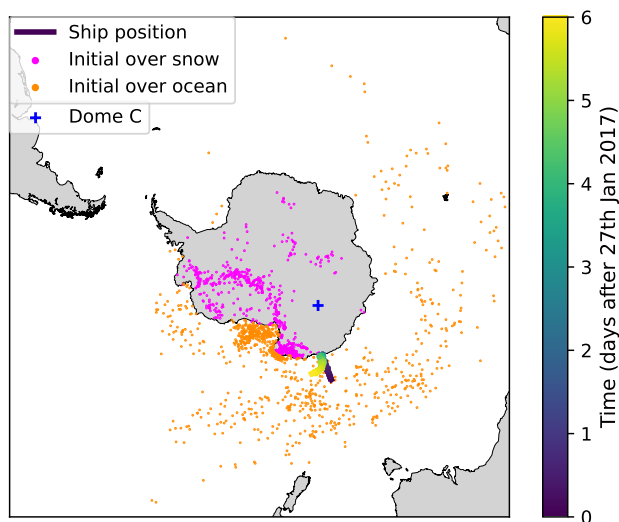


Figure 2. Map with the position of the ship (colored line) during the study period, the initial locations of the modelled air parcels (dots), and the location of Dome C (blue cross).

272 Along the trajectory, the specific humidity and isotopic composition of the parcel
 273 can change due to the surface flux and cloud formation. The surface flux will only af-
 274 fect the parcel if it resides in the ABL. Assuming a well-mixed ABL with a height-constant
 275 vapour density, the moisture flux into or out of the parcel (J_a) due to the surface flux

276 (J) is computed as

$$J_a = J \frac{d_a}{d_{ABL}}, \quad (1)$$

277 where $d_a = 1$ m and d_{ABL} are the depths of the air parcel and ABL, respectively. The
 278 specific humidity in *Model Air Parcel* agrees approximately with that in the trajectory
 279 data set (Figure S3 in the Supporting Information). Considering all data points from
 280 the initialization of the air parcels to the arrival at the ship, the specific humidity in *Model*
 281 *Air Parcel* is characterized by a RMSE of 0.6 g kg⁻¹ and a correlation coefficient of $\rho =$
 282 0.94 when compared with the trajectory data set. Comparing only the values at the fi-
 283 nal position of the air parcels (i.e., at the ship) with the trajectory data set, specific hu-
 284 midity tends to be underestimated with RMSE = 0.9 g kg⁻¹ and $\rho = 0.45$.

285 In the case of snow sublimation, the isotopic composition of the surface flux is taken
 286 from *Model Sublimation*. In all other cases (ocean evaporation, condensation, or vapour
 287 deposition), the isotopic composition of the surface flux depends and feeds back on that
 288 of the air parcel (Text S3 in the Supporting Information). To guarantee an accurate feed-
 289 back, the time step needs to be small enough, especially if the vapour mass taken up or
 290 removed from the air parcel is in the same order of magnitude as the vapour mass con-
 291 tained in the parcel. Therefore, the effects of ocean evaporation, condensation, or vapour
 292 deposition are computed step-wise by dividing each 3-h time step into 32 sub-intervals
 293 of equal length. This value was justified using an example situation, for which the num-
 294 ber of sub-intervals was continuously increased by a factor of two until the isotopic com-
 295 position of the parcel at the end of the 3-h step changed by less than 1 %. We assume
 296 that there is no sea ice during the 6-day period in austral summer.

297 Isotopic fractionation during cloud formation is calculated using the classic Rayleigh
 298 distillation model with equilibrium fractionation (Jouzel & Merlivat, 1984; Sinclair et
 299 al., 2011). It assumes that the liquid or solid water phase is removed immediately after
 300 its formation, i.e., the cloud water precipitates immediately. The equilibrium fraction-
 301 ation factors used in the Rayleigh model are computed as in Sinclair et al. (2011), ac-
 302 counting for mixed-phase clouds with a gradual, linear shift from the vapour-liquid to
 303 the vapour-ice transition as the air temperature decreases from 0° C to -20° C. Changes
 304 in air density along the trajectory influence the vapour mass contained in the parcel as
 305 they imply exchange of air with the surrounding atmosphere. The model assumes that
 306 this exchange of air does not have a direct effect on the isotopic composition of the par-
 307 cel.

308 3 Results and Discussion

309 As the model only accounts for equilibrium fractionation in most phase change pro-
 310 cesses, the simulated dynamics of $\delta^{18}\text{O}$ and δD are very similar. Therefore, we only present
 311 results for $\delta^{18}\text{O}$.

312 3.1 Comparison of Modelled and Measured Vapour Isotopic Composi- 313 tions

314 Figure 3 compares the ensemble averaged vapour $\delta^{18}\text{O}$ of the air parcels with the
 315 measurements on the ship close to the Mertz glacier. We show the baseline simulations
 316 using the relationship of Stenni16 to parameterize the snowfall isotopic composition in
 317 *Model Sublimation*. Similar to the measurements, the modelled vapour $\delta^{18}\text{O}$ at the ship
 318 is approximately -15‰ in the beginning and at the end of the investigated 6-day pe-
 319 riod and reaches a minimum of approximately -39‰ in the middle of the period. The
 320 simulation considering equilibrium fractionation (Run E) leads to slightly more depleted
 321 vapour isotopic compositions in the middle of the period, compared to the simulation
 322 neglecting fractionation during snow sublimation (Run N). At other times, the vapour
 323 isotopic composition is identical for both model runs. Overall, both runs achieve a sim-

324 ilar agreement with the measurements with the same root-mean-square error (RMSE)
 325 of 5.2‰ and similar Pearson correlation coefficients of 0.82 (Run E) and 0.80 (Run N).

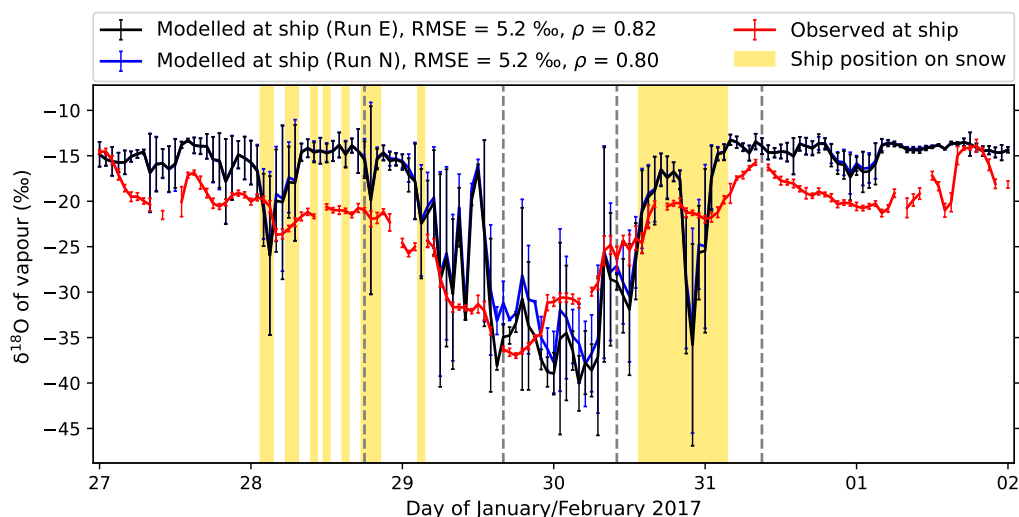


Figure 3. Modelled and measured $\delta^{18}\text{O}$ of atmospheric water vapour at the ship close to the Mertz glacier from 27th January to 1st February 2017. We show the modelled ensemble averages and standard deviations for multiple air parcels in the baseline simulations. The measurements represent 1-h mean values and standard deviations. In the legend, root-mean-square errors (RMSE) and Pearson correlation coefficients (ρ) are specified. The yellow shading indicates times when the ship was located in a grid cell modelled as snow surface; at the other times, the ship was in a grid cell treated as ocean surface. The vertical grey dashed lines indicate times analyzed in Figure 6.

326 In the first two and last two days of the period, the modelled $\delta^{18}\text{O}$ is generally more
 327 enriched than the measured one with an average difference of 4‰. Possible reasons may
 328 be (i) a bias in the initial isotopic composition of air parcels over the ocean due to the
 329 global closure assumption or a bias in the surface water $\delta^{18}\text{O}$; (ii) the neglect of kinetic
 330 fractionation during cloud formation; (iii) the neglect of mixing of air masses with dif-
 331 ferent isotopic compositions, e.g., at weather fronts; and (iv) the simple assumption that
 332 the vapour mass exchanged between the atmosphere and the surface is homogeneously
 333 distributed in the ABL (Equation 1). This last assumption does not account for the fact
 334 that the air and vapour densities decrease with height and that the air in the ABL may
 335 not be perfectly mixed, especially in a stable ABL.

336 The largest mismatch between the model and the measurements is found on 29th
 337 January at 12:00 and 30th January at 22:00 when the modelled time series shows two
 338 strong peaks. The first (second) peak overestimates (underestimates) the measured $\delta^{18}\text{O}$
 339 by approximately 15‰. Apart from the aforementioned shortcomings of the model, the
 340 coarse spatial resolution may contribute to the temporary mismatch as the coastline is
 341 not accurately represented. During the first (second) peak, the ship was located in a grid
 342 cell treated as ocean (snow) surface (yellow shading in Figure 3). Consequently, the model
 343 may overestimate (underestimate) the time spent by the air parcels in the marine ABL
 344 shortly before arriving at the ship. If an air parcel with a strongly depleted $\delta^{18}\text{O}$ value
 345 reaches the coast and takes up moisture from the liquid ocean surface, the isotopic sig-
 346 nature of the parcel can change abruptly as the $\delta^{18}\text{O}$ value of the evaporation flux can
 347 be depleted or enriched compared to the ocean water (Equation S13 in the Supporting

348 Information). Furthermore, sea ice may cover a part of the ocean close to the Antarctic
 349 coast even in austral summer, which is neglected in the model. Additionally, the ABL
 350 height provided with the trajectory data set may not always be accurate, which influ-
 351 ences the modelled time period and magnitude of moisture exchange between the air parcels
 352 and the surface. Although there are some hours with a large model-measurement mis-
 353 match, the model is able to reproduce the general trend and timing of the vapour de-
 354 pletion event on 29th and 30th January 2017.

355 3.2 Sensitivity of the Isotopic Composition of the Air Parcels with Re- 356 spect to That of Snowfall

357 It is important to note that changing the snowfall isotopic composition in *Model*
 358 *Sublimation* does not affect the isotopic composition of the air parcels during cloud for-
 359 mation. The isotopic composition of snowfall is only used to estimate that of surface snow,
 360 which determines that of the sublimation flux and influences the initial isotopic compo-
 361 sition of the air parcels. Figure 4 shows how the modelled $\delta^{18}\text{O}$ at the ship changes when
 362 assuming different snowfall δ -temperature relationships in Run E (Equations S7 to S9).
 363 Differences in the $\delta^{18}\text{O}$ time series are mainly visible in the middle of the study period,
 364 suggesting that many air parcels are initialized over snow or influenced by sublimation
 365 at this time. The snowfall δ -temperature relationship of FA06 leads to a less pronounced
 366 minimum of -34‰ in the vapour $\delta^{18}\text{O}$ time series, compared with the baseline simu-
 367 lation using the relationship of Stenni16. On the contrary, the snowfall δ -temperature
 368 relationship of Landais12 leads to the most pronounced $\delta^{18}\text{O}$ minimum of -45‰ . The
 369 best agreement with the measurements is obtained for the baseline simulation (RMSE =
 370 5.2‰ , $\rho = 0.82$) although the agreement is still reasonable for the simulations using
 371 the relationships of FA06 (RMSE = 5.3‰ , $\rho = 0.80$) and Landais12 (RMSE = 5.7‰ ,
 372 $\rho = 0.82$). The generalization of a site-dependent, idealized δ -temperature relationship
 373 for snowfall is a strong simplification in the model and contributes to deviations between
 374 the model and the measurements. Nevertheless, the associated sensitivity of the vapour
 375 $\delta^{18}\text{O}$ is small enough to draw useful conclusions about the dominant processes driving
 376 the isotopic signal.

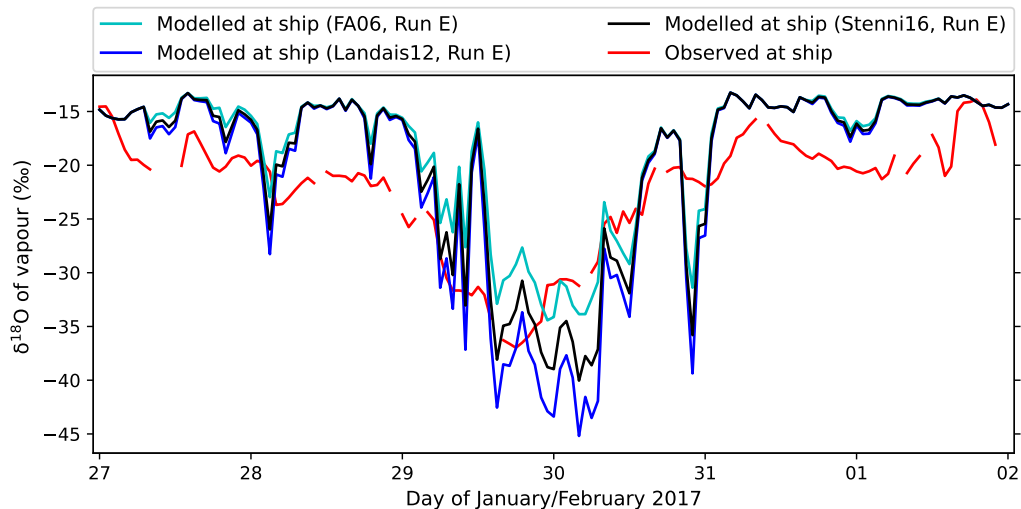


Figure 4. Effect of different snowfall δ -temperature relationships assumed in *Model Sublimation* on the modelled $\delta^{18}\text{O}$ of atmospheric water vapour at the ship in Run E. Modelled ensemble averages are compared with measured 1-h averages.

3.3 Drivers of the Vapour Isotopic Composition

Previous studies at other coastal polar sites have found distinct isotopic signatures for air masses advected from the ocean and those advected from the ice sheet (e.g., Kopec et al., 2014; Kurita et al., 2016a, 2016b). Therefore, it is a plausible hypothesis that shifts between such air masses largely explain the observed isotope dynamics close to the Mertz glacier. The more depleted isotopic composition of vapour over the ice sheet is generally thought to result from the distillation effect of cloud formation. However, snow sublimation including isotopic fractionation also influences the variability of the vapour isotopic composition. As the ocean is often a strong vapour source, the distance between the ship and the ice sheet may play an important role. In the marine boundary layer, a strong vertical humidity gradient, typically associated with cold air advection over a relatively warm ocean surface, leads to strong evaporation with enhanced equilibrium and kinetic fractionation. This effect can cause differences of several ‰ in the vapour $\delta^{18}\text{O}$ between cold and warm sectors of extratropical cyclones but it is unlikely to explain a large decrease of more than 10‰ (Thurnherr et al., 2021). We now investigate which of the aforementioned drivers play a dominant role in our case study.

On the first day and during most of the last two days of the study period, the ship moved towards and away from the ice sheet, respectively (Figure 2). Due to a longer distance to the ice sheet, it is likely that recent ocean evaporation caused the relatively enriched vapour $\delta^{18}\text{O}$ at this time. From 28th January 2017, 02:00, to 31st January 2017, 06:00, the ship stayed in close proximity to the ice sheet. In this phase, the $\delta^{18}\text{O}$ remained relatively enriched for one day and then dropped to very depleted values. The fact that only the most depleted $\delta^{18}\text{O}$ values in the time series are sensitive with respect to assumptions in *Model Sublimation* (Figures 3 and 4) is consistent with the hypothesis that processes over the ocean drove the vapour isotopic composition in the first and last two days of the period while processes over the Antarctic Ice Sheet influenced the isotopic signature in the middle of the period. Moreover, the small differences between Runs E and N demonstrate that isotopic fractionation during snow sublimation can only explain a very small part of the minimum in the $\delta^{18}\text{O}$ time series.

The initial isotopic composition of the air parcels can influence the model results, especially if the time between initialization and arrival at the ship is short. Air parcels initialized over the ocean start their trajectories with a fairly uniform $\delta^{18}\text{O}$ between approximately -15‰ and -11‰ (Figure 5a). These initial values are similar to the final isotopic composition modelled at the ship during the first two and last two days of the investigation period, suggesting that ocean evaporation is an important driver. As expected, air parcels initialized over snow have more variable and more depleted initial $\delta^{18}\text{O}$ values than those initialized over ocean. Interestingly, there are almost always some air parcels that are initialized over snow and the range of their initial $\delta^{18}\text{O}$ values remains similar throughout the period (approximately -70‰ to -40‰). However, when the most depleted $\delta^{18}\text{O}$ values are observed at the ship, almost all air parcels are initialized over snow. This fact supports the hypothesis that the air masses originate from the interior of the ice sheet at this time.

To assess the importance of different moisture exchange processes along the trajectories, we show in Figure 5b the ensemble-averaged total change of vapour mass in an air parcel due to specific processes. Except in the middle of the study period, moisture uptake from the ocean and moisture removal due to cloud formation clearly have the largest impact on the moisture budget of the air parcels. As expected, the magnitude of these moisture exchanges largely reflects the varying travel times of the air parcels and, in particular, the amount of time spent in the marine ABL (Figure 5c). Only in the middle of the study period, moisture uptake due to snow sublimation becomes the dominant term in the moisture budget of the parcels while the time spent in the marine ABL is close to zero. Although the parcels experience very little cloud formation at this time, the distillation effect of cloud formation may still be responsible for the very depleted $\delta^{18}\text{O}$ val-

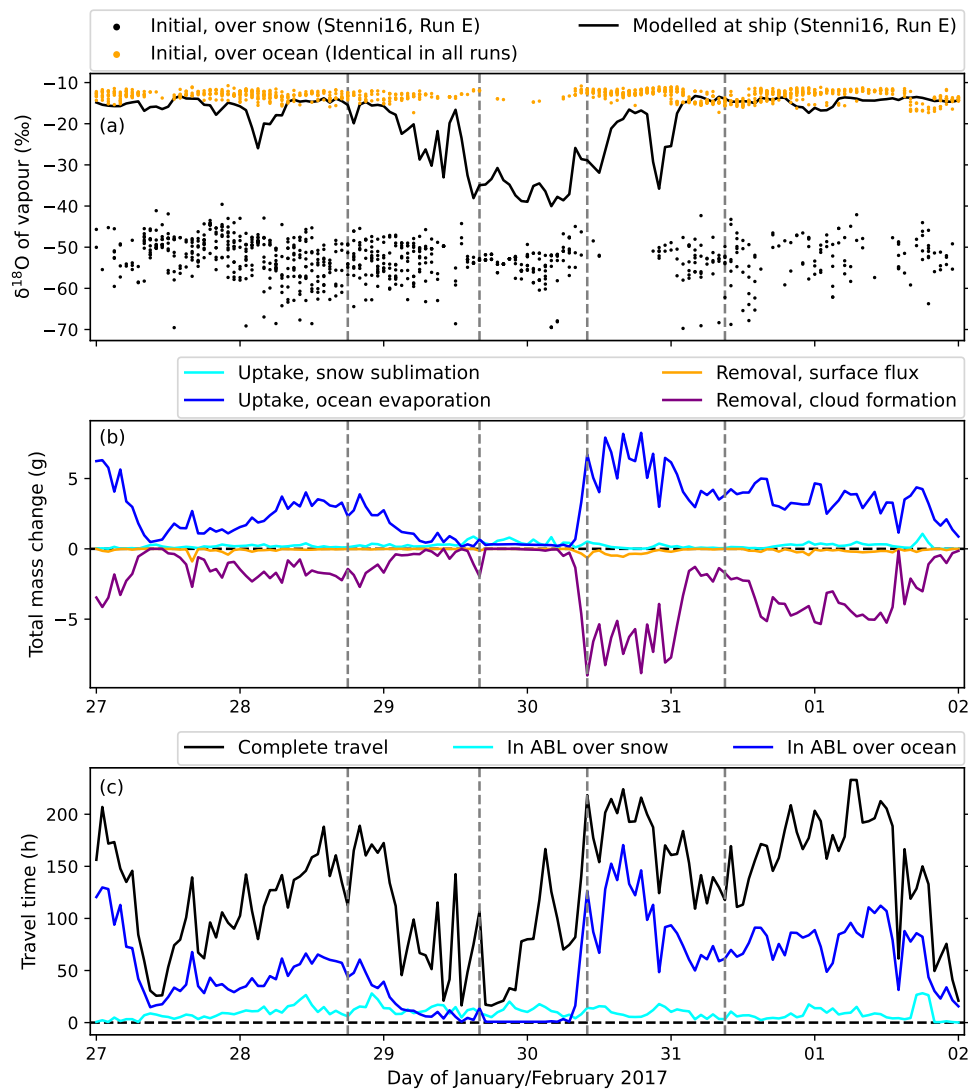


Figure 5. (a) Comparison between initial $\delta^{18}\text{O}$ of individual air parcels and ensemble-averaged final $\delta^{18}\text{O}$ in Run E; (b) Ensemble average of the total change of vapour mass in an air parcel due to different processes between initialization and arrival at the ship; (c) Average travel time of the air parcels and average times spent in the boundary layers (ABLs) over snow and ocean. The vertical grey dashed lines indicate times analyzed in Figure 6.

430 uses as this effect is reflected by the temperature dependence of the initial isotopic composition of the air parcels over snow. Vapour removal due to the surface flux is generally the smallest term in the moisture budget and most of the time negligible. Overall, 431 432 433 Figures 3–5 show that the air masses with the most depleted $\delta^{18}\text{O}$ values originate from the ice sheet and their isotopic signature is influenced by snow sublimation. This isotopic signature seems to only reach the ship if the air masses spend little time in the marine ABL shortly before their arrival such that ocean evaporation cannot overwrite the signature. 434 435 436 437

438 To better understand which drivers act in which sections of the air parcel trajectories, we present trajectory maps for four different arrival times in Figure 6. The ar- 439

440 rival times include situations with relatively enriched and depleted $\delta^{18}\text{O}$ values while the
 441 ship was close to the ice sheet and the ensemble averaged travel time of the air parcels
 442 was at least 4 days. Similar maps indicating locations where the parcels reside in the ABL
 443 can be found in Figure S4 in the Supporting Information. Figures 6a and 6d show similar
 444 situations leading to relatively enriched $\delta^{18}\text{O}$ values at the ship. In both situations,
 445 the air parcels travel some distance in the marine ABL parallel to the Antarctic coast
 446 before arriving at the ship. Almost half of the air parcels are initialized over the ice sheet
 447 and exhibit strongly depleted $\delta^{18}\text{O}$ values around -50‰ until they enter the marine ABL.
 448 Due to ocean evaporation, the $\delta^{18}\text{O}$ of the air parcels quickly increases and reaches val-
 449 ues comparable to those of parcels initialized over the ocean.

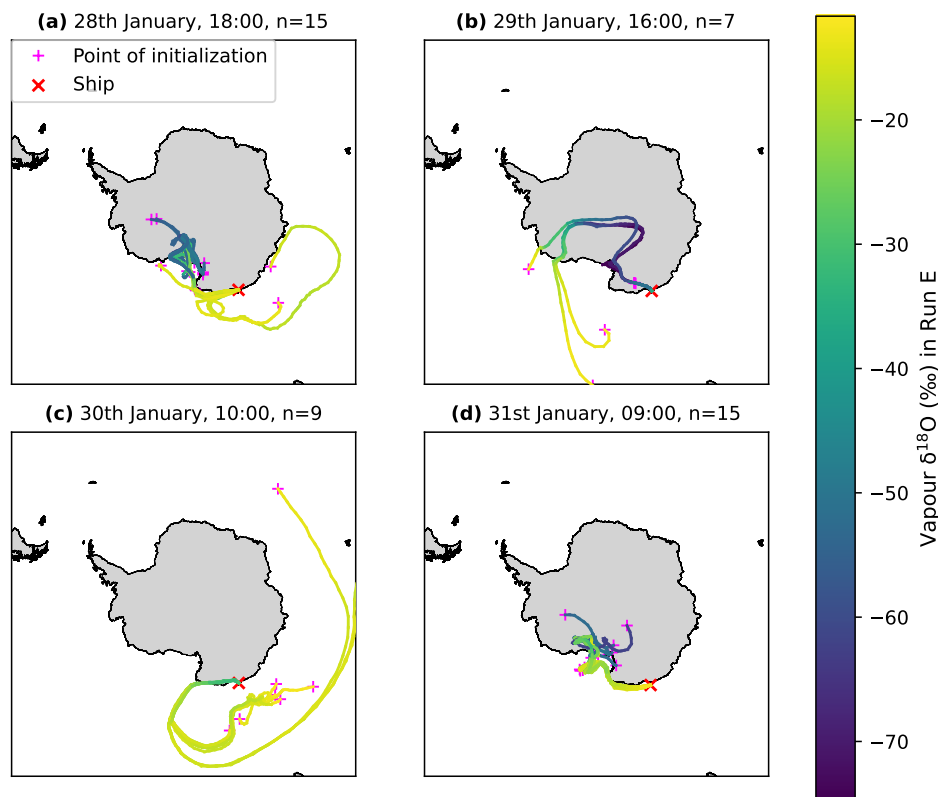


Figure 6. Vapour $\delta^{18}\text{O}$ along air parcel trajectories in the baseline simulation of Run E for four different times of arrival at the ship (grey dashed lines in Figures 3 and 5). The number of trajectories is denoted by n . Trajectories arriving at the ship at a lower height are plotted on top of other trajectories.

450 Figure 6b refers to a situation with one of the most depleted $\delta^{18}\text{O}$ values measured
 451 at the ship. Four of seven air parcels are initialized over the ice sheet and take a direct
 452 and short route to the ship where they only take up moisture from the ocean in the last
 453 time step. Their final $\delta^{18}\text{O}$ values are similar to those of the other three parcels that are
 454 initialized over the ocean and travel over the interior of the ice sheet before taking the
 455 same final route as the parcels initialized over snow. While the parcels are lifted over the
 456 ice sheet, their isotopic composition becomes increasingly depleted due to the distilla-
 457 tion effect of cloud formation and reaches extreme $\delta^{18}\text{O}$ values of approximately -60‰ to
 458 -75‰ . Only towards the end of the trajectories as the parcels move over the escarpment
 459 zone of the ice sheet, they enter the ABL over snow (Figure S4b). At this time, approx-
 460 imately 20 h before the arrival at the ship, snow sublimation adds vapour with a rela-

461 tively enriched $\delta^{18}\text{O}$ value to the parcels (Figure 7). The sublimation flux in the escarp-
 462 ment zone is relatively enriched in heavy SWIs compared to the air parcels because their
 463 isotopic composition was shaped at higher and colder levels over the interior of the ice
 464 sheet. Additionally, the parcel isotopic composition is particularly sensitive with respect
 465 to moisture uptake after most of the initial vapour mass was removed from parcels due
 466 to cloud formation. As a consequence, the moisture uptake in the escarpment zone in-
 467 creases the isotopic composition of the parcels abruptly. This increase caused by sub-
 468 limation is similarly strong as another increase in the last time step, when the parcels
 469 reach the ocean and take up moisture from the water surface.

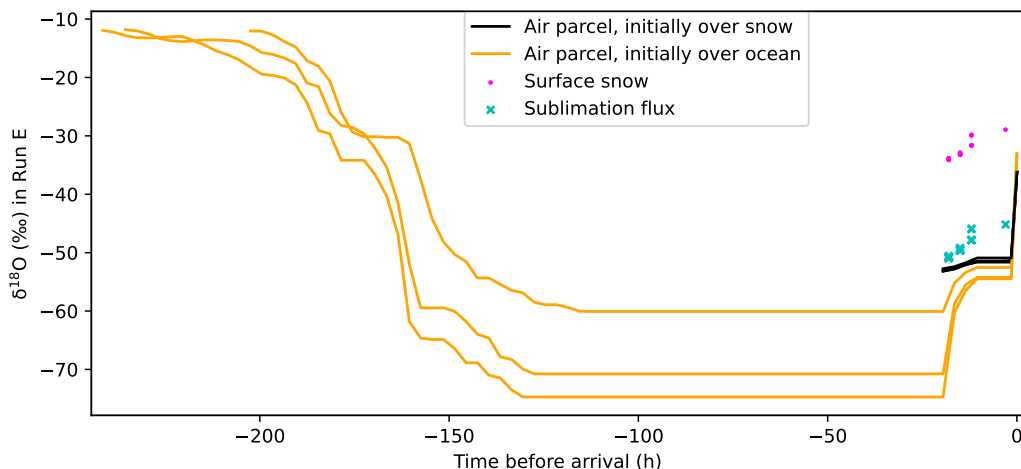


Figure 7. Vapour $\delta^{18}\text{O}$ as a function of time for the air parcel trajectories arriving at the ship on 29th January, 16:00, in the baseline simulation of Run E (corresponding to Figure 6b). The points and crosses show $\delta^{18}\text{O}$ values of the surface snow and sublimation flux, respectively, at locations where the air parcels reside in the ABL over snow.

470 The situation shown in Figure 6c leads to an intermediate $\delta^{18}\text{O}$ at the ship. All
 471 air parcels start their trajectories over the ocean and finally travel over the coastal zone
 472 of the ice sheet. Already over the ocean, cloud formation and condensation at the sur-
 473 face begin to decrease the $\delta^{18}\text{O}$ of the parcels. As soon as the parcels reach the ice sheet,
 474 their $\delta^{18}\text{O}$ continues to decrease because snow sublimation adds vapour with a more de-
 475 pleted $\delta^{18}\text{O}$ value to the air parcels. In this situation, the sublimation flux is more de-
 476 pleted in heavy SWIs compared to the parcels because the latter carry the isotopic sig-
 477 nature of processes over the ocean.

478 4 Conclusions

479 We developed a Lagrangian isotope model with the aim to reproduce and explain
 480 the vapour $\delta^{18}\text{O}$ time series measured on the ACE ship close to the Mertz glacier in a
 481 6-day period in austral summer 2017. The vapour mass and isotopic composition of air
 482 parcels was modelled along trajectories between an initial location in the ABL and the
 483 final location in the ABL at the ship. While isotope effects of cloud formation and ocean
 484 evaporation were represented with common approaches (classic Rayleigh distillation model
 485 and Craig-Gordon formula, respectively), the effect of snow sublimation was estimated
 486 using a novel approach, considering changes of the isotopic composition in a multi-layer
 487 snowpack due to snowfall, sublimation, and vapour deposition.

488 Similar to the measured values, the modelled vapour $\delta^{18}\text{O}$ at the ship reaches a pro-
489 nounced minimum value of -39‰ in the middle of the study period. The RMSE of the
490 baseline simulation amounts to 5.2‰ , which is reasonable considering the model lim-
491 itations such as the neglect of kinetic fractionation in phase change processes apart from
492 ocean evaporation and the neglect of mixing of air masses with different isotopic com-
493 positions. Our analysis confirms the hypothesis that the relatively enriched $\delta^{18}\text{O}$ values
494 are associated with air masses advected from the ocean whereas the strongly depleted
495 $\delta^{18}\text{O}$ values are caused by direct advection of air masses from the Antarctic Ice Sheet.
496 This result is consistent with similar observations at other coastal polar sites in the lit-
497 erature. As expected, cloud formation leads to very depleted vapour isotopic composi-
498 tions over the ice sheet. Snow sublimation can also significantly modify the isotopic com-
499 position of the air parcels depending on their origin. For example, air parcels originat-
500 ing from high levels over the interior of the ice sheet may carry a strongly depleted iso-
501 topic signature to the escarpment zone of the ice sheet and then experience an abrupt
502 and strong enrichment in heavy SWIs due to a relatively enriched sublimation flux. How-
503 ever, the model options of considering or neglecting equilibrium fractionation during sub-
504 limation play a minor role. A critical factor for the vapour $\delta^{18}\text{O}$ at the ship is the time
505 that the air parcels spend in the marine ABL shortly before arriving at the ship because
506 ocean evaporation can quickly overwrite their isotopic signature.

507 Our modelling approach could be adapted for a study similar to Helsen et al. (2006)
508 to simulate the vertical isotope profile in snow pits using backward trajectories for events
509 of snow accumulation at an Antarctic site and deriving the isotopic composition of lo-
510 cal snowfall from that of the air parcels. In contrast to the model of Helsen et al. (2006),
511 our model accounts for the post-depositional effects of snow sublimation and vapour de-
512 position. However, further improvements in our model such as the parameterization of
513 kinetic fractionation during cloud formation and a more sophisticated vapour transport
514 mechanism in the snowpack may be important for this purpose. Moreover, the deposi-
515 tion of drifting and blowing snow can contribute to snow accumulation and influence the
516 isotopic composition of surface snow. To understand the latter effect, fundamental re-
517 search is needed as the isotopic composition of drifting and blowing snow particles may
518 be altered by sublimation, which has not been studied so far.

519 Acknowledgements

520 We thank Iris Thurnherr and Franziska Aemisegger for providing inspiration for
521 this study as well as feedback. We thank Sonja Wahl for valuable comments on the manuscript.
522 The team of the ACE campaign is acknowledged for providing the measurement data.
523 Funding for the ACE campaign was provided by the ACE Foundation, Ferring Pharma-
524 ceuticals, RFBR (grant no. 18-55-16001), Swiss Data Science Center (grant no. 17-02)
525 and the RCN project FARLAB. Funding for this study was provided by the Swiss-European
526 Mobility Programme and the Swiss National Science Foundation (grant 200020-179130).

527 The authors declare that they have no conflict of interest.

528 Open Research

529 Model results were generated using Copernicus Climate Change Service informa-
530 tion [2021] available at <https://doi.org/10.24381/cds.adbb2d47> (Hersbach et al., 2018).
531 The air parcel trajectories were downloaded from <https://doi.org/10.5281/zenodo.4031705>
532 (Thurnherr, Wernli, & Aemisegger, 2020). The calibrated isotope measurements from
533 the ACE campaign were downloaded from <https://doi.org/10.5281/zenodo.3250790> (Thurnherr
534 & Aemisegger, 2020). Validation data from the Dome C site containing $\delta^{18}\text{O}$ of surface
535 snow and atmospheric vapour were retrieved from [https://doi.org/10.5194/tc-12-1745-](https://doi.org/10.5194/tc-12-1745-2018-supplement)
536 [2018-supplement](https://doi.org/10.5194/acp-16-8521-2016-supplement) and <https://doi.org/10.5194/acp-16-8521-2016-supplement>, respectively
537 (Casado et al., 2016, 2018). The python programming code and the main model output

538 including the data shown in the figures are available at
 539 <https://drive.switch.ch/index.php/s/ObsiN3bmBGagk9P> (This data will be published
 540 in a repository at the end of the peer review process). The figures were made with Mat-
 541 plotlib version 3.5.1, available under the Matplotlib license at <https://matplotlib.org/>.

542 References

- 543 Akers, P. D., Kopec, B. G., Mattingly, K. S., Klein, E. S., Causey, D., & Welker,
 544 J. M. (2020). Baffin Bay sea ice extent and synoptic moisture transport drive
 545 water vapor isotope ($\delta^{18}\text{O}$, $\delta^2\text{H}$, and deuterium excess) variability in coastal
 546 northwest Greenland. *Atmospheric Chemistry and Physics*, *20*(22), 13929–
 547 13955.
- 548 Bonne, J.-L., Behrens, M., Meyer, H., Kipfstuhl, S., Rabe, B., Schönicke, L., ...
 549 Werner, M. (2019). Resolving the controls of water vapour isotopes in the
 550 Atlantic sector. *Nature Communications*, *10*(1), 1632.
- 551 Bréant, C., Dos Santos, C. L., Agosta, C., Casado, M., Fourré, E., Goursaud, S.,
 552 ... others (2019). Coastal water vapor isotopic composition driven by katabatic
 553 wind variability in summer at Dumont d'Urville, coastal East Antarctica.
 554 *Earth and Planetary Science Letters*, *514*, 37–47.
- 555 Casado, M., Landais, A., Masson-Delmotte, V., Genthon, C., Kerstel, E., Kassi, S.,
 556 ... Cermak, P. (2016). Continuous measurements of isotopic composition
 557 of water vapour on the East Antarctic Plateau. *Atmospheric Chemistry and*
 558 *Physics*, *16*, 8521–8538.
- 559 Casado, M., Landais, A., Picard, G., Münch, T., Laepple, T., Stenni, B., ... others
 560 (2018). Archival processes of the water stable isotope signal in East Antarctic
 561 ice cores. *The Cryosphere*, *12*(5), 1745–1766.
- 562 Christner, E., Kohler, M., & Schneider, M. (2017). The influence of snow sublimation
 563 and meltwater evaporation on δD of water vapor in the atmospheric
 564 boundary layer of central Europe. *Atmospheric Chemistry & Physics*, *17*(2).
- 565 Ciais, P., & Jouzel, J. (1994). Deuterium and oxygen 18 in precipitation: Isotopic
 566 model, including mixed cloud processes. *Journal of Geophysical Research: At-*
 567 *mospheres*, *99*(D8), 16793–16803.
- 568 Craig, H. (1961). Standard for reporting concentrations of deuterium and oxygen-18
 569 in natural waters. *Science*, *133*(3467), 1833–1834.
- 570 Craig, H., & Gordon, L. I. (1965). *Stable Isotopes in Oceanographic Studies and*
 571 *Paleotemperatures* (E. Tongiorgi, Ed.). Spoleto: Consiglio nazionale delle
 572 ricerche, Laboratorio de geologia nucleare Pisa.
- 573 Cuffey, K. M., & Steig, E. J. (1998). Isotopic diffusion in polar firn: implications for
 574 interpretation of seasonal climate parameters in ice-core records, with emphasis
 575 on central Greenland. *Journal of Glaciology*, *44*(147), 273–284.
- 576 Dar, S. S., Ghosh, P., Swaraj, A., & Kumar, A. (2020). Craig–Gordon model valida-
 577 tion using stable isotope ratios in water vapor over the Southern Ocean. *Atmo-*
 578 *spheric Chemistry and Physics*, *20*(19), 11435–11449.
- 579 Dütsch, M., Pfahl, S., Meyer, M., & Wernli, H. (2018). Lagrangian process attri-
 580 bution of isotopic variations in near-surface water vapour in a 30-year regional
 581 climate simulation over Europe. *Atmospheric Chemistry and Physics*, *18*(3),
 582 1653–1669.
- 583 Ebner, P. P., Steen-Larsen, H. C., Stenni, B., Schneebeli, M., & Steinfeld, A. (2017).
 584 Experimental observation of transient $\delta^{18}\text{O}$ interaction between snow and ad-
 585 vective airflow under various temperature gradient conditions. *The Cryosphere*,
 586 *11*, 1733–1743.
- 587 ECMWF. (2016). IFS Documentation CY41R2 - Part IV: Physical Processes. In *IFS*
 588 *Documentation CY41R2*. doi: 10.21957/tr5rv27xu
- 589 Elliot, T. (2014). *Environmental tracers*. Multidisciplinary Digital Publishing Insti-
 590 tute.

- 591 EPICA community members. (2004). Eight glacial cycles from an Antarctic ice core.
592 *Nature*, *429*(6992), 623–628.
- 593 Friedman, I., Benson, C., & Gleason, J. (1991). Isotopic changes during snow meta-
594 morphism. In *Stable isotope geochemistry: a tribute to Samuel Epstein* (pp.
595 211–221).
- 596 Fujita, K., & Abe, O. (2006). Stable isotopes in daily precipitation at Dome Fuji,
597 East Antarctica. *Geophysical Research Letters*, *33*(18).
- 598 Gat, J. R., Mook, W. G., & Meijer, H. (2001). Environmental isotopes in the hydro-
599 logical cycle: Principles and Applications. *Technical Documents in Hydrology*,
600 *2*(39).
- 601 Gat, J. R., Shemesh, A., Tziperman, E., Hecht, A., Georgopoulos, D., & Basturk, O.
602 (1996). The stable isotope composition of waters of the eastern Mediterranean
603 Sea. *Journal of Geophysical Research: Oceans*, *101*(C3), 6441–6451.
- 604 Grootes, P., Steig, E., & Stuiver, M. (1994). Taylor Ice Dome study 1993–1994: An
605 ice core to bedrock. *Antarctic Journal of the United States*, *29*, 79–81.
- 606 Helsen, M., Van de Wal, R., & Van den Broeke, M. (2007). The isotopic composition
607 of present-day Antarctic snow in a Lagrangian atmospheric simulation. *Journal*
608 *of Climate*, *20*(4), 739–756.
- 609 Helsen, M., Van de Wal, R., Van den Broeke, M., As, D. v., Meijer, H., & Reijmer,
610 C. (2005). Oxygen isotope variability in snow from western Dronning Maud
611 Land, Antarctica and its relation to temperature. *Tellus B: Chemical and*
612 *Physical Meteorology*, *57*(5), 423–435.
- 613 Helsen, M., Van de Wal, R., Van den Broeke, M., Masson-Delmotte, V., Meijer,
614 H., Scheele, M., & Werner, M. (2006). Modeling the isotopic composition of
615 Antarctic snow using backward trajectories: Simulation of snow pit records.
616 *Journal of Geophysical Research: Atmospheres*, *111*(D15).
- 617 Hersbach, H., Bell, B., Berrisford, P., Biavati, G., Horányi, A., Muñoz Sabater, J.,
618 ... others (2018). *ERA5 hourly data on single levels from 1979 to present*.
619 *Copernicus Climate Change Service (C3S) Climate Data Store (CDS)*. [Data
620 set]. (Accessed on 15-10-2021) doi: 10.24381/cds.bd0915c6
- 621 Hoffmann, G., Jouzel, J., & Masson, V. (2000). Stable water isotopes in atmospheric
622 general circulation models. *Hydrological Processes*, *14*(8), 1385–1406.
- 623 Horita, J., Rozanski, K., & Cohen, S. (2008). Isotope effects in the evaporation of
624 water: a status report of the Craig–Gordon model. *Isotopes in Environmental*
625 *and Health Studies*, *44*(1), 23–49.
- 626 Hughes, A. G., Wahl, S., Jones, T. R., Zühr, A., Hörhold, M., White, J. W. C., &
627 Steen-Larsen, H. C. (2021). The role of sublimation as a driver of climate
628 signals in the water isotope content of surface snow: laboratory and field ex-
629 perimental results. *The Cryosphere*, *15*(10), 4949–4974.
- 630 Jafari, M., Gouttevin, I., Couttet, M., Wever, N., Michel, A., Sharma, V., ... Lehn-
631 ing, M. (2020). The Impact of Diffusive Water Vapor Transport on Snow
632 Profiles in Deep and Shallow Snow Covers and on Sea Ice. *Frontiers in Earth*
633 *Science*, *8*, 249.
- 634 Johnsen, S. J., Dahl-Jensen, D., Gundestrup, N., Steffensen, J. P., Clausen, H. B.,
635 Miller, H., ... White, J. (2001). Oxygen isotope and palaeotemperature
636 records from six Greenland ice-core stations: Camp Century, Dye-3, GRIP,
637 GISP2, Renland and NorthGRIP. *Journal of Quaternary Science: Published*
638 *for the Quaternary Research Association*, *16*(4), 299–307.
- 639 Joussaume, S., Sadourny, R., & Jouzel, J. (1984). A general circulation model of wa-
640 ter isotope cycles in the atmosphere. *Nature*, *311*(5981), 24–29.
- 641 Jouzel, J., & Merlivat, L. (1984). Deuterium and oxygen 18 in precipitation: Mod-
642 eling of the isotopic effects during snow formation. *Journal of Geophysical Re-*
643 *search: Atmospheres*, *89*(D7), 11749–11757.
- 644 Jouzel, J., Vimeux, F., Caillon, N., Delaygue, G., Hoffmann, G., Masson-Delmotte,
645 V., & Parrenin, F. (2003). Magnitude of isotope/temperature scaling for in-

- 646 terpretation of central Antarctic ice cores. *Journal of Geophysical Research:*
647 *Atmospheres*, 108(D12).
- 648 Koeniger, P., Leibundgut, C., Link, T., & Marshall, J. D. (2010). Stable isotopes
649 applied as water tracers in column and field studies. *Organic Geochemistry*,
650 41(1), 31–40.
- 651 Kopec, B., Lauder, A., Posmentier, E., & Feng, X. (2014). The diel cycle of wa-
652 ter vapor in west Greenland. *Journal of Geophysical Research*, 119(15), 9386–
653 9399.
- 654 Krinner, G., & Werner, M. (2003). Impact of precipitation seasonality changes on
655 isotopic signals in polar ice cores: a multi-model analysis. *Earth and Planetary*
656 *Science Letters*, 216(4), 525–538.
- 657 Kumar, B., & Nachiappan, R. P. (1999). On the sensitivity of Craig and Gordon
658 Model for the estimation of the isotopic composition of lake evaporates. *Water*
659 *Resources Research*, 35(5), 1689–1691.
- 660 Kurita, N., Hirasawa, N., Koga, S., Matsushita, J., Steen-Larsen, H. C., Masson-
661 Delmotte, V., & Fujiyoshi, Y. (2016a). Identification of Air Masses Responsible
662 for Warm Events on the East Antarctic Coast. *SOLA*, 12(0), 307–313.
- 663 Kurita, N., Hirasawa, N., Koga, S., Matsushita, J., Steen-Larsen, H. C., Masson-
664 Delmotte, V., & Fujiyoshi, Y. (2016b). Influence of large-scale atmospheric
665 circulation on marine air intrusion toward the East Antarctic coast. *Geophysi-*
666 *cal Research Letters*, 43(17), 9298–9305.
- 667 Landais, A., Ekaykin, A., Barkan, E., Winkler, R., & Luz, B. (2012). Seasonal varia-
668 tions of ^{17}O -excess and d-excess in snow precipitation at Vostok station, East
669 Antarctica. *Journal of Glaciology*, 58(210), 725–733.
- 670 LeGrande, A. N., & Schmidt, G. A. (2006). Global gridded data set of the oxy-
671 gen isotopic composition in seawater. *Geophysical Research Letters*, 33(12),
672 L12604.
- 673 Lorius, C., Merlivat, L., Jouzel, J., & Pourchet, M. (1979). A 30,000-yr isotope cli-
674 matic record from Antarctic ice. *Nature*, 280(5724), 644–648.
- 675 Majoube, M. (1970). Fractionation factor of ^{18}O between water vapour and ice.
676 *Nature*, 226(5252), 1242–1242.
- 677 Majoube, M. (1971). Fractionnement en oxygène 18 et en deutérium entre l’eau et
678 sa vapeur. *J. Chim. Phys.*, 68, 1423–1436.
- 679 Masson-Delmotte, V., Hou, S., Ekaykin, A., Jouzel, J., Aristarain, A., Bernardo,
680 R., . . . others (2008). A review of antarctic surface snow isotopic composi-
681 tion: Observations, atmospheric circulation, and isotopic modeling. *Journal of*
682 *climate*, 21(13), 3359–3387.
- 683 Merlivat, L. (1978). Molecular diffusivities of H_2^{16}O , HD^{16}O , and H_2^{18}O in gases. *J.*
684 *Chem. Phys.*, 69, 2864–2871.
- 685 Merlivat, L., & Jouzel, J. (1979). Global climatic interpretation of the deuterium-
686 oxygen 18 relationship for precipitation. *Journal of Geophysical Research:*
687 *Oceans*, 84(C8), 5029–5033.
- 688 Merlivat, L., & Nief, G. (1967). Fractionnement isotopique lors des changements
689 d’état solide-vapeur et liquide-vapeur de l’eau à des températures inférieures à
690 0°C . *Tellus*, 19(1), 122–127.
- 691 Neumann, T. A., & Waddington, E. D. (2004). Effects of firn ventilation on isotopic
692 exchange. *Journal of Glaciology*, 50(169), 183–194.
- 693 Noone, D., & Sturm, C. (2010). Comprehensive dynamical models of global and re-
694 gional water isotope distributions. In *Isoscapes* (pp. 195–219). Springer.
- 695 Pfahl, S., Wernli, H., & Yoshimura, K. (2012). The isotopic composition of pre-
696 cipitation from a winter storm – a case study with the limited-area model
697 COSMO_{iso}. *Atmospheric Chemistry and Physics*, 12(3), 1629–1648.
- 698 Sigmund, A., Dujardin, J., Comola, F., Sharma, V., Huwald, H., Melo, D. B., . . .
699 Lehning, M. (2021). Evidence of Strong Flux Underestimation by Bulk
700 Parametrizations During Drifting and Blowing Snow. *Boundary-Layer Meteo-*

- 701 *rology*.
- 702 Sinclair, K. E., Marshall, S. J., & Moran, T. A. (2011). A Lagrangian approach to
703 modelling stable isotopes in precipitation over mountainous terrain. *Hydrologi-*
704 *cal Processes*, 25(16), 2481–2491.
- 705 Sokratov, S. A., & Golubev, V. N. (2009). Snow isotopic content change by sublima-
706 tion. *Journal of Glaciology*, 55(193), 823–828.
- 707 Sprenger, M., & Wernli, H. (2015). The LAGRANTO Lagrangian analysis tool-
708 version 2.0. *Geoscientific Model Development*, 8(8), 2569–2586.
- 709 Stenni, B., Scarchilli, C., Masson-Delmotte, V., Schlosser, E., Ciardini, V., Dreossi,
710 G., . . . others (2016). Three-year monitoring of stable isotopes of precipitation
711 at Concordia Station, East Antarctica. *The Cryosphere*, 10(5), 2415–2428.
- 712 Thurnherr, I., & Aemisegger, F. (2020). *Calibrated data of stable water isotope*
713 *measurements in water vapour at 13.5 m a.s.l., made in the austral summer of*
714 *2016/2017 around the Southern Ocean during the Antarctic Circumnavigation*
715 *Expedition (ACE)*. [Data set]. Zenodo. doi: 10.5281/zenodo.3250790
- 716 Thurnherr, I., Hartmuth, K., Jansing, L., Gehring, J., Boettcher, M., Gorodetskaya,
717 I., . . . Aemisegger, F. (2021). The role of air–sea fluxes for the water vapour
718 isotope signals in the cold and warm sectors of extratropical cyclones over the
719 Southern Ocean. *Weather and Climate Dynamics*, 2(2), 331–357.
- 720 Thurnherr, I., Kozachek, A., Graf, P., Weng, Y., Bolshiyarov, D., Landwehr, S., . . .
721 others (2020). Meridional and vertical variations of the water vapour isotopic
722 composition in the marine boundary layer over the Atlantic and Southern
723 Ocean. *Atmospheric Chemistry and Physics*, 20(9), 5811–5835.
- 724 Thurnherr, I., Wernli, H., & Aemisegger, F. (2020). *10-day backward trajectories*
725 *from ECMWF analysis data along the ship track of the Antarctic Circumnav-*
726 *igation Expedition in austral summer 2016/2017*. [Data set]. Zenodo. doi:
727 10.5281/zenodo.4031705
- 728 Town, M. S., Warren, S. G., Walden, V. P., & Waddington, E. D. (2008). Effect
729 of atmospheric water vapor on modification of stable isotopes in near-surface
730 snow on ice sheets. *Journal of Geophysical Research: Atmospheres*, 113(D24).
- 731 Wahl, S., Steen-Larsen, H. C., Reuder, J., & Hörhold, M. (2021). Quantifying
732 the stable water isotopologue exchange between the snow surface and lower
733 atmosphere by direct flux measurements. *Journal of Geophysical Research:*
734 *Atmospheres*, 126(13).
- 735 Wernli, B. H., & Davies, H. C. (1997). A Lagrangian-based analysis of extratropical
736 cyclones. I: The method and some applications. *Quarterly Journal of the Royal*
737 *Meteorological Society*, 123(538), 467–489.

Figure 1.

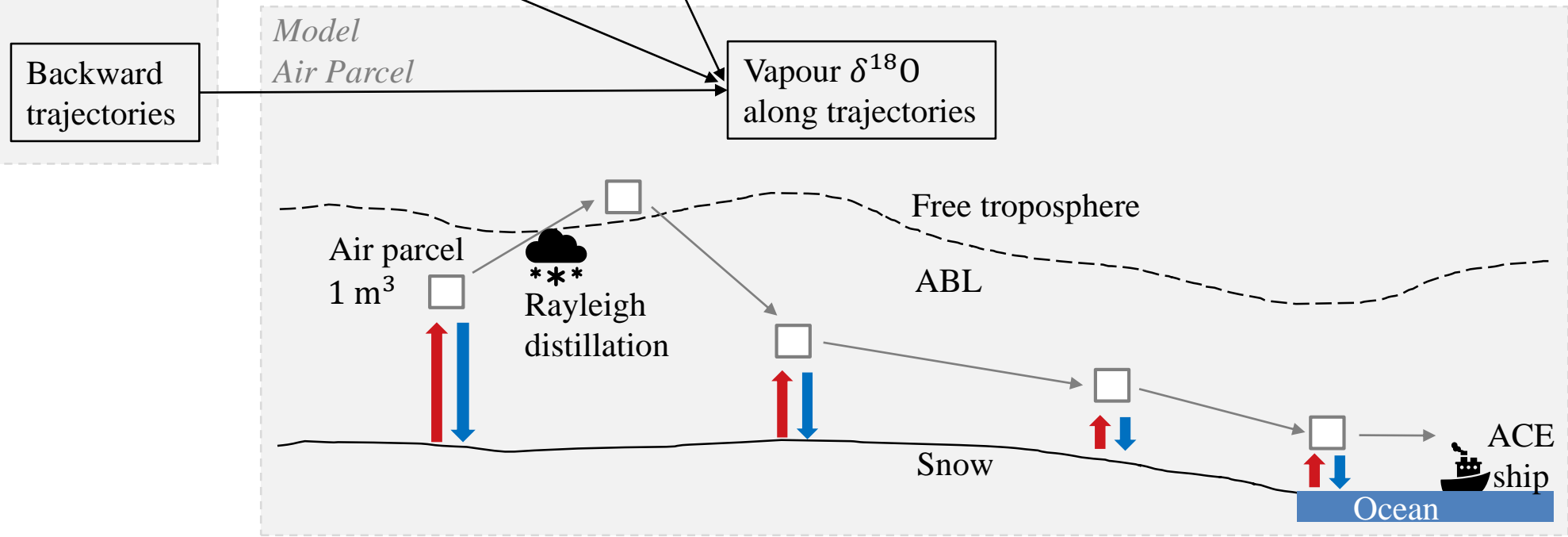
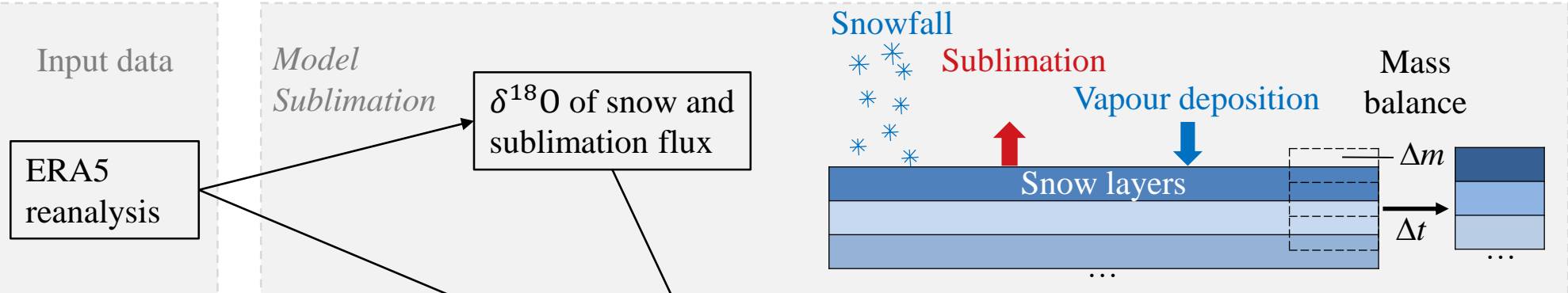


Figure 2.

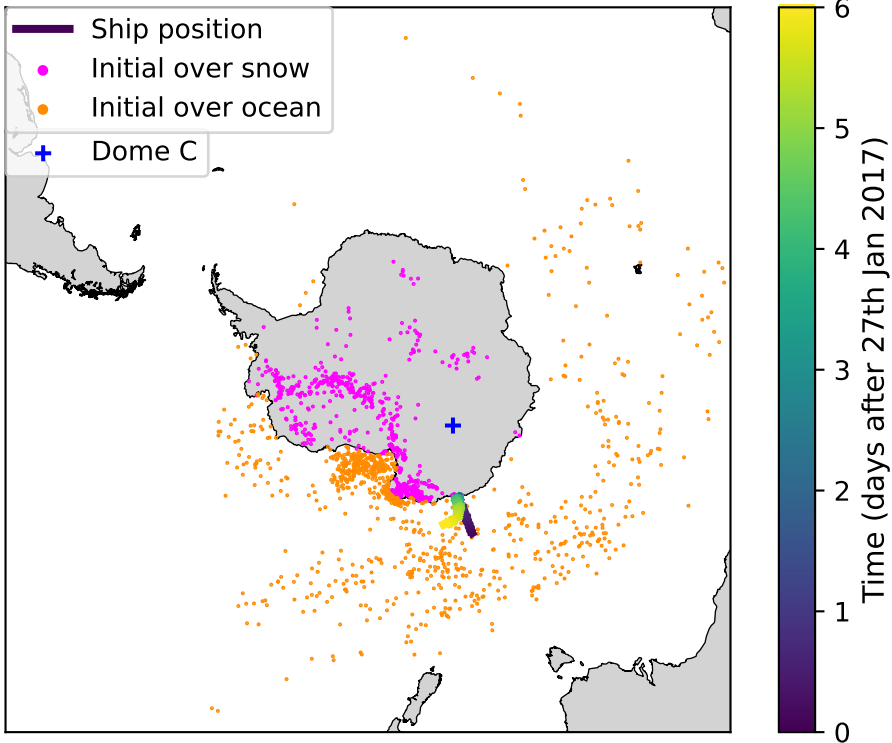


Figure 3.

—+— Modelled at ship (Run E), RMSE = 5.2 ‰, $\rho = 0.82$
—+— Modelled at ship (Run N), RMSE = 5.2 ‰, $\rho = 0.80$

—+— Observed at ship
■ Ship position on snow

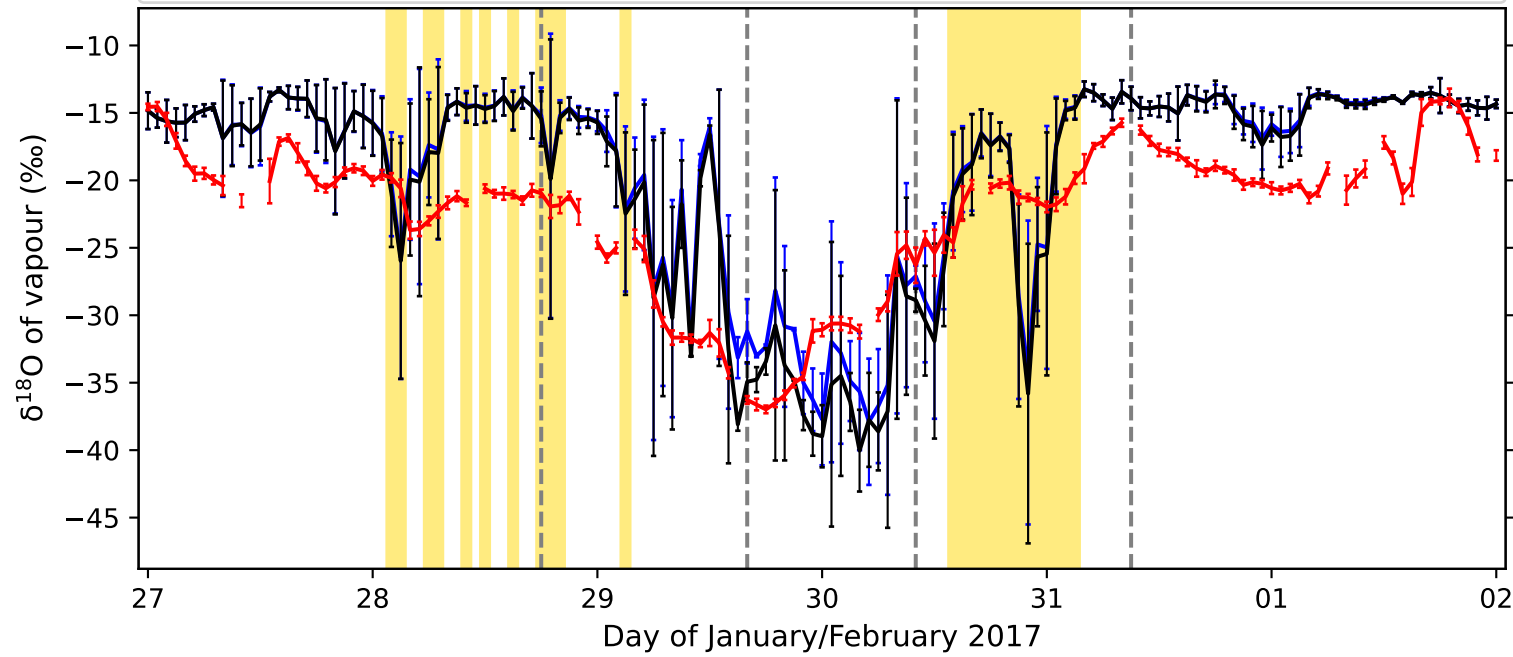


Figure 4.

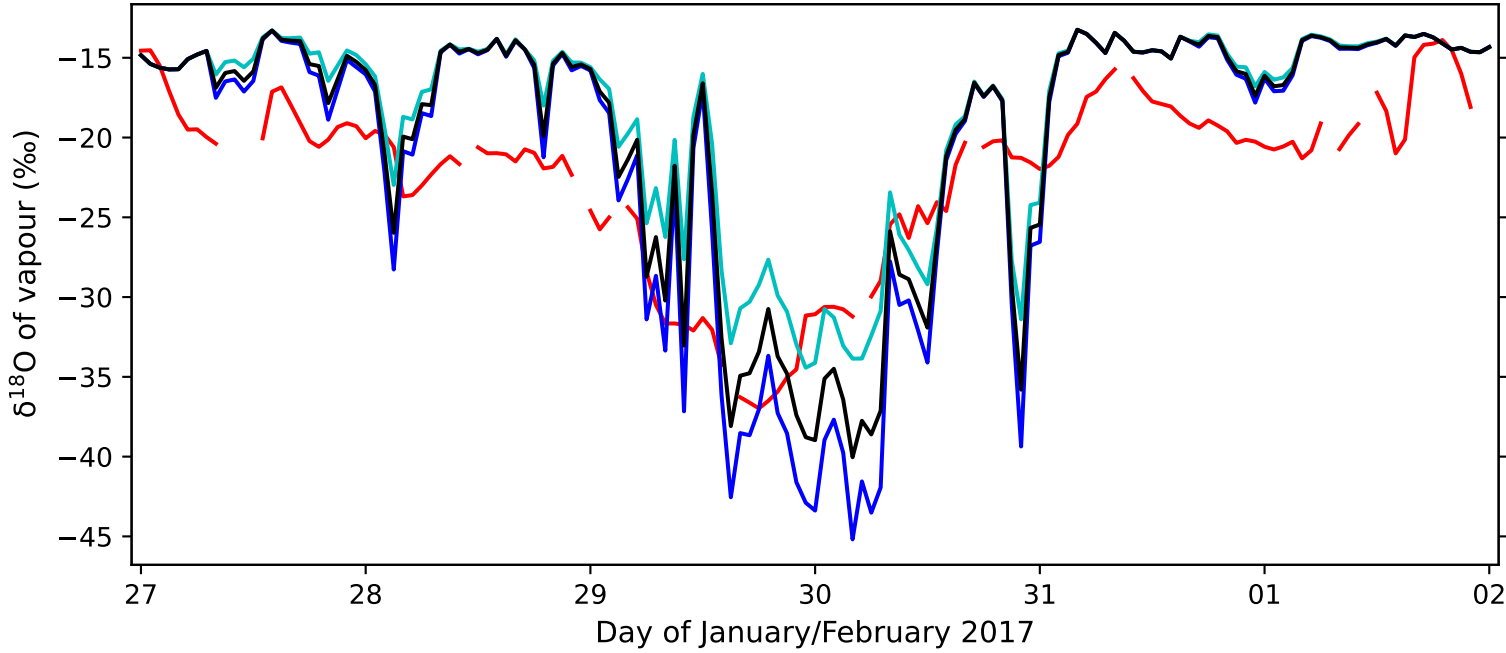


Figure 5.

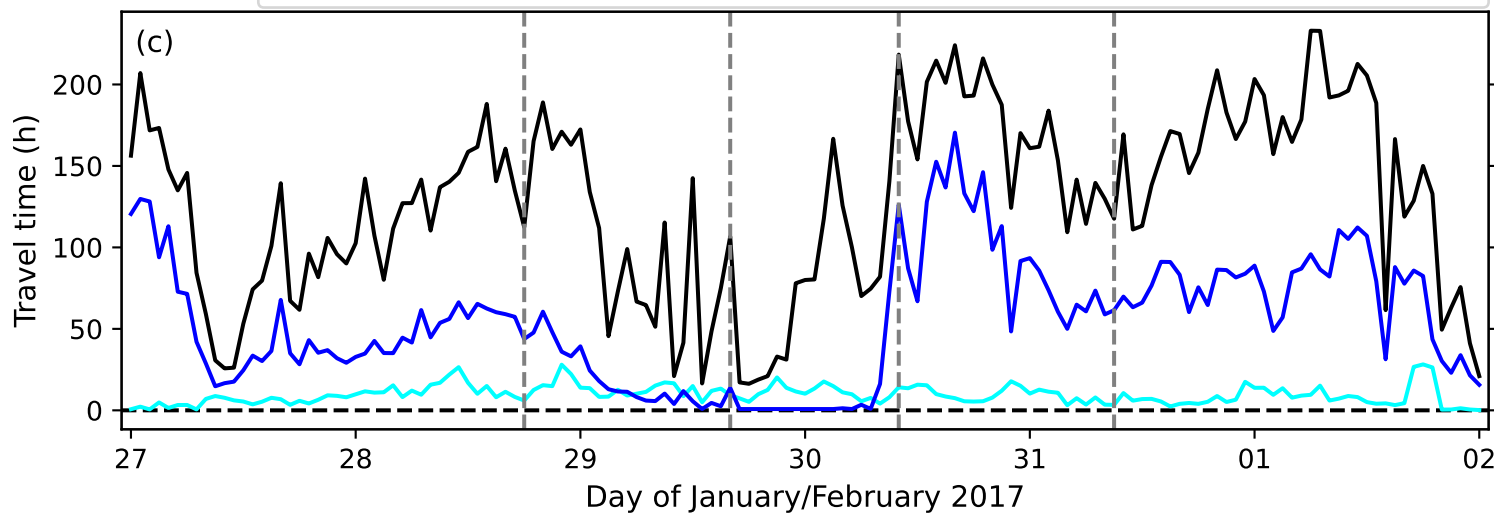
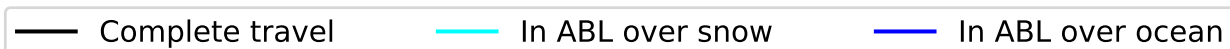
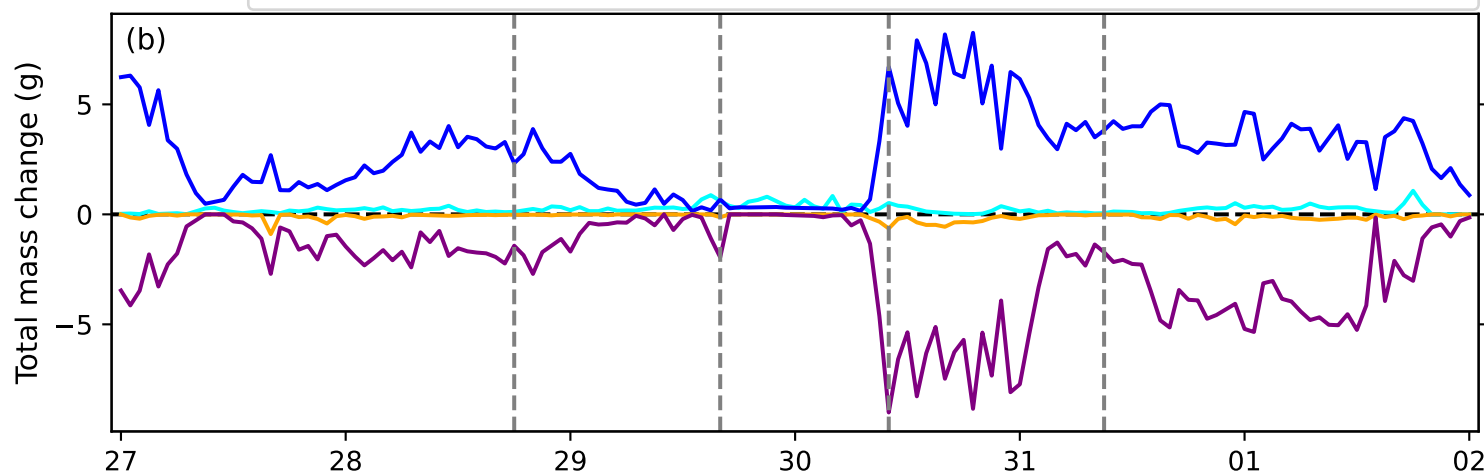
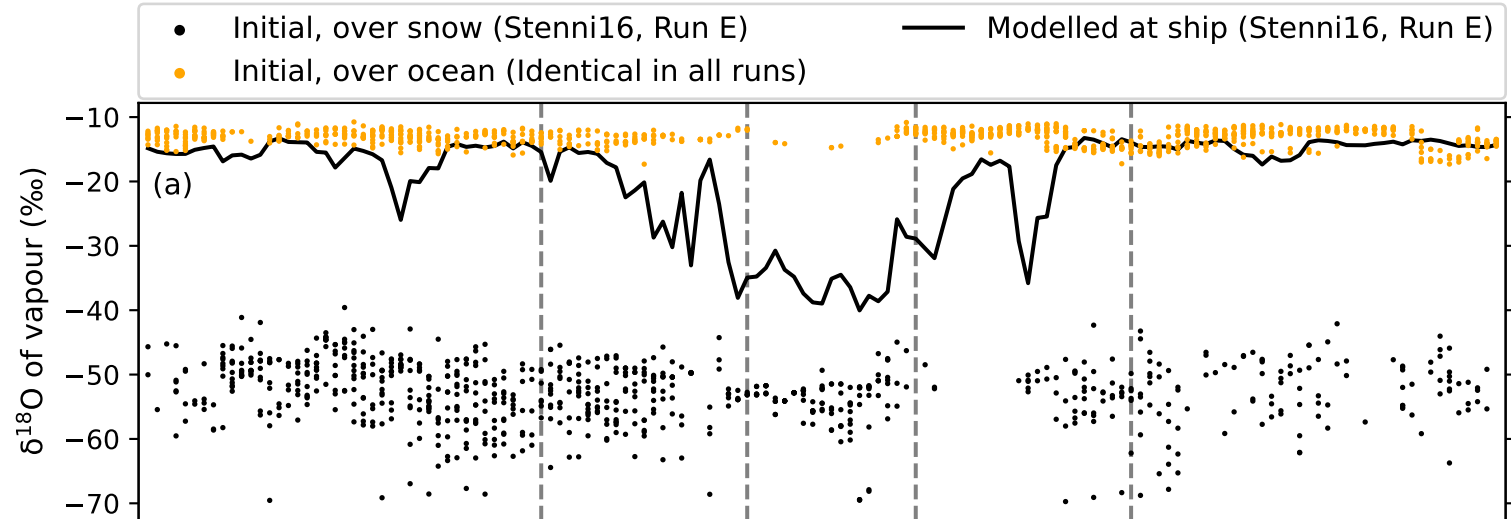
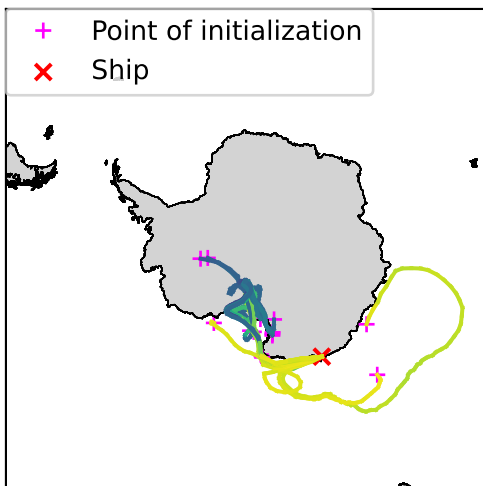
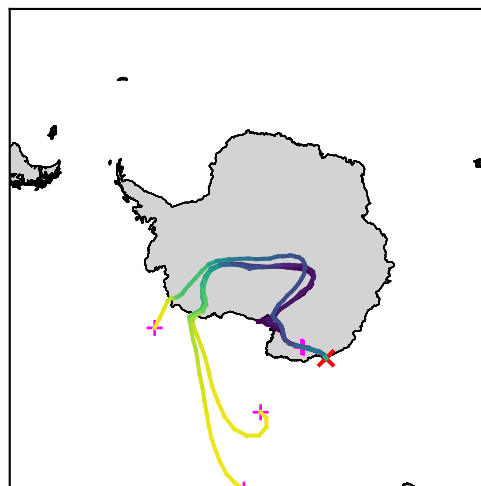


Figure 6.

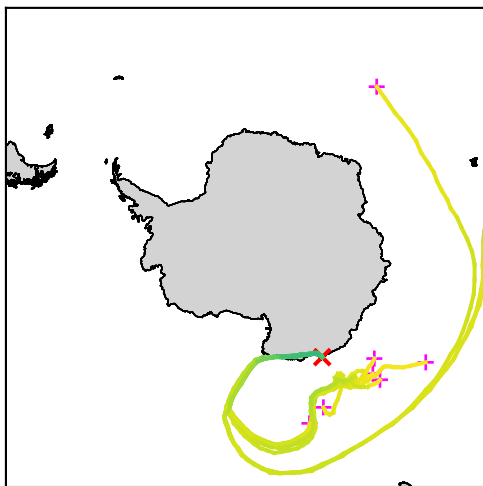
(a) 28th January, 18:00, n=15



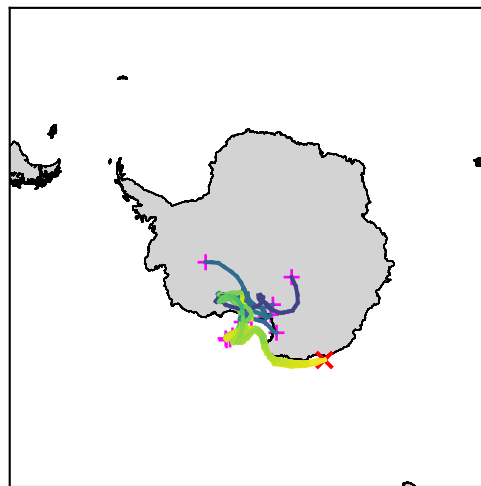
(b) 29th January, 16:00, n=7



(c) 30th January, 10:00, n=9



(d) 31st January, 09:00, n=15



Vapour $\delta^{18}\text{O}$ (‰) in Run E

-20

-30

-40

-50

-60

-70

Figure 7.

